

Arbitrarily High-order Unconditionally Energy Stable Schemes for Gradient Flow Models Using the Scalar Auxiliary Variable Approach

Yuezheng Gong ^{*}, Jia Zhao [†] and Qi Wang [‡]

Abstract

In this paper, we propose a novel family of high-order numerical schemes for the gradient flow models based on the scalar auxiliary variable (SAV) approach, which is named the high-order scalar auxiliary variable (HSAV) method. The newly proposed schemes could be shown to reach arbitrarily high order in time while preserving the energy dissipation law without any restriction on the time step size (i.e., unconditionally energy stable). The HSAV strategy is rather general that it does not depend on the specific expression of the effective free energy, such that it applies to a class of thermodynamically consistent gradient flow models arriving at semi-discrete high-order energy-stable schemes. We then employ the Fourier pseudospectral method for spatial discretization. The fully discrete schemes are also shown to be unconditionally energy stable. Furthermore, we present several numerical experiments on several widely-used gradient flow models, to demonstrate the accuracy, efficiency and unconditionally energy stability of the HSAV schemes. The numerical results verify that the HSAV schemes can reach the expected order of accuracy, and it allows a much larger time step size to reach the same accuracy than the standard SAV schemes.

1 Introduction

The dynamics of many dissipative systems could be driven by an effective free energy that is decreasing with time, where the decreasing path is controlled by a certain dissipation mechanism [32, 33, 51, 46]. To study such dynamics in the macroscopic level, a gradient flow model is usually used. In general, consider the state variables $\Phi(\mathbf{x}, t)$ for a dissipative system on the domain Ω . The evolution (kinetic) equation for $\Phi(\mathbf{x}, t)$ could be formulated as [39]

$$\partial_t \Phi(\mathbf{x}, t) = \mathcal{G} \frac{\delta F}{\delta \Phi}, \quad (1.1)$$

where \mathcal{G} is a negative semi-definite differential or integral operator which might depend on the state variables Φ . Here F is the effective free energy, and $\frac{\delta F}{\delta \Phi}$ is the variational derivative of F with respect to the state variable Φ , called the chemical potential. For instance, if $F = F(\Phi, \nabla \Phi)$, the chemical potential would be $\frac{\delta F}{\delta \Phi} = \frac{\partial F}{\partial \Phi} - \nabla \cdot \left(\frac{\partial F}{\partial \nabla \Phi} \right)$. In this paper, we consider periodic boundary conditions for simplicity of notations.

^{*}College of Science, Nanjing University of Aeronautics and Astronautics, Nanjing 210016, China; Email: gongyuezheng@nuaa.edu.cn.

[†]Department of Mathematics & Statistics, Utah State University, Logan, UT, USA; email: jia.zhao@usu.edu.

[‡]Department of Mathematics, University of South Carolina, Columbia, SC, 29208, USA; email: qwang@math.sc.edu.

The system (1.1) is a general gradient flow model, which has an intrinsic energy dissipation law. Actually, if we take inner product of (1.1) with the chemical potential $\frac{\delta F}{\delta \Phi}$, we have the energy dissipation law

$$\frac{dF}{dt} = \int_{\Omega} \left(\frac{\delta F}{\delta \Phi} \right)^T \mathcal{G} \frac{\delta F}{\delta \Phi} d\mathbf{x} \leq 0, \quad (1.2)$$

thanks to the negative semi-definite property of \mathcal{G} .

Note that the gradient flow model could be specified once the triple (Φ, \mathcal{G}, F) is given. It turns out many dissipative PDE models could be classified as a special case of the general gradient flow model in (1.1). For instance, if we specify the state variable as ϕ , the mobility as $\mathcal{G} = -M$ (with M a positive constant) and the free energy as $F = \int_{\Omega} \left[\frac{1}{2} |\nabla \phi|^2 + \frac{1}{4\varepsilon^2} (\phi^2 - 1)^2 \right] d\mathbf{x}$ (with ε a free parameter), the general gradient flow model (1.1) reduces to the well-known Allen-Cahn equation [1]

$$\partial_t \phi = -M \left(-\Delta \phi + \frac{1}{\varepsilon^2} (\phi^3 - \phi) \right). \quad (1.3)$$

If we use the same free energy and specify the mobility as $\mathcal{G} = M\Delta$, we end up with the well-known Cahn-Hilliard equation [4]

$$\partial_t \phi = M\Delta \left(-\Delta \phi + \frac{1}{\varepsilon^2} (\phi^3 - \phi) \right). \quad (1.4)$$

Moreover, there are many more examples which could be cast as special cases of (1.1), including molecular beam epitaxy (MBE) growth models [42, 6], phase field crystal models [19], dendritic crystal growth models [44], multiphase models [3, 27]. For a detailed discussion, readers can refer to [51] and the references therein.

Along with the broad applications of gradient flow models, many accurate, efficient and stable numerical schemes are developed for longtime dynamic simulations of the dissipative systems. As the dynamics follow a specified trace of dissipating the effective free energy, one essential indication of stable numerical schemes is to preserve the energy dissipation law at the discrete level. A numerical scheme that possesses such property is known as energy stable. If such numerical stability does not have any restrictions on the time step size, it is then usually named unconditionally energy stable. In practice, energy dissipation preserving schemes are always desirable as they mimic the physical structures of the original problem and thus perform excellent numerical stability even with large marching time step size. Due to its practical significance, a large number of innovative work have been developed, please see [10, 42, 43, 40, 36, 20, 2, 31, 25, 26, 8, 22, 48, 47] and the references therein. However, most of these existing schemes have strict restrictions on \mathcal{G} and F , i.e., they only work for particular gradient flow models. Recently, Yang et al. [50, 51, 17, 18, 24] propose an energy quadratization (EQ) approach to bypass the restrictions and obtain linear energy stable schemes, which can be applied for almost all gradient flow problems. Shen et al. [39, 38] further extend the EQ idea to develop the scalar auxiliary variable (SAV) approach, where the resulting linear schemes can be solved quickly by the fast Fourier transform (FFT). The primary idea of both EQ and SAV is to introduce some auxiliary variables to reformulate a gradient flow model into an equivalent form, such that the effective free energy is a quadratic functional in the reformulated equivalent system. Then linear and unconditionally energy stable schemes could be constructed easily for the reformulated system, which in turn solves the original gradient flow model. Due to the generality of the EQ and SAV approaches, they have been applied for many existing gradient flow models [48, 47, 50, 39, 38, 6, 21].

However, most of the existing energy stable schemes are up to second-order accurate in time. There is little work on developing higher order energy stable schemes. Since

gradient flow models usually require longtime dynamic simulations to reach the steady state, high order accurate energy stable schemes are always desirable, which makes large marching steps practical while preserving the accuracy. Several seminal works on developing high-order energy-stable numerical schemes include [41, 15]. In this paper, we take advantage of the SAV idea [39, 38] to develop arbitrarily high-order energy-stable numerical schemes for gradient flow models in two steps: firstly, we utilize the SAV technique to transform the gradient flow model into an equivalent form. The transformed equivalent system turns out to have a quadratic free energy functional along with a modified energy dissipation law; secondly, we exploit the structure-preserving Gaussian collocation and RK methods to derive high-order scalar auxiliary variable (HSAV) schemes, which are proved rigorously to preserve the discrete modified energy dissipation law. Note that the newly proposed high-order schemes overcome all the drawbacks of the convex-splitting RK scheme in [41]. For instance, by utilizing the SAV technique, our approach does not have any restrictions on specific forms of the mobility \mathcal{G} and effective free energy F , making it applicable to all the existing gradient flow models. Moreover, by employing the Gaussian collocation method, our approach can reach arbitrarily high-order accuracy in time with optimal RK stages.

The rest of this paper is organized as follows. In Section 2, we will present the general gradient flow model and its equivalent reformulation based on the SAV approach. In Section 3, we derive the high-order time discretization for the reformulated system and prove its unconditional energy stability. In Section 4, we use the Fourier pseudo-spectral method for spatial discretization to arrive at fully discrete schemes, which are shown to be unconditionally energy stable as well. Several numerical examples are presented in Section 5. In the end, we give the concluding remarks.

2 Gradient Flow Models and Their SAV Reformulation

In this section, we start from general gradient flow models and apply the SAV approach to derive an equivalent form, which has a quadratic energy functional and an energy dissipation law for the new system. We call this approach energy quadratization reformulation (or SAV reformulation). The EQ/SAV reformulation for the gradient flow models provides an elegant platform for developing arbitrarily high-order unconditionally energy stable schemes, which is the major focus of this paper.

2.1 General gradient flow models

Consider the material domain Ω with enough regularity on the boundary. The L^2 inner product and its norm are defined as $\forall f, g \in L^2(\Omega)$, $(f, g) = \int_{\Omega} fg d\mathbf{x}$ and $\|f\|_2 = \sqrt{(f, f)}$, respectively. For simplicity, we consider a single state variable ϕ . The dynamics of ϕ is driven by an effective free energy or Lyapunov function F and a negative semi-definite mobility operator \mathcal{G} . Thus the gradient flow model is formulated as

$$\partial_t \phi = \mathcal{G} \frac{\delta F}{\delta \phi}. \quad (2.1)$$

The generic form of the effective free energy F could be written as

$$F = \frac{1}{2}(\mathcal{L}\phi, \phi) + (g, 1), \quad (2.2)$$

where \mathcal{L} is a linear, self-adjoint operator, and g is a potential functional that might depend on ϕ and its low order spatial derivatives. For instance, given the widely used

Ginzburg-Landau free energy functional for the two phase immersible materials

$$F = \int_{\Omega} \gamma \left[\frac{\varepsilon}{2} |\nabla \phi|^2 + \frac{1}{\varepsilon} \phi^2 (1 - \phi)^2 \right] d\mathbf{x}, \quad (2.3)$$

where γ is the surface tension, and ε is the interfacial thickness, we can cast

$$\mathcal{L} = -\gamma\varepsilon\Delta + \gamma_0, \quad g(\phi) = \frac{\gamma}{\varepsilon} \phi^2 (1 - \phi)^2 - \frac{\gamma_0}{2} \phi^2, \quad (2.4)$$

where γ_0 is a non-negative constant (stabilization parameter [6]), by assuming periodic boundary conditions or other proper boundary conditions such that the boundary integral terms are canceled out.

With the specific form of effective free energy F in (2.2), the gradient flow model (2.1) could be rewritten as

$$\partial_t \phi = \mathcal{G} \left(\mathcal{L} \phi + \frac{\delta g}{\delta \phi} \right). \quad (2.5)$$

Here we note that \mathcal{L} is self-adjoint and \mathcal{G} is negative semi-definite, i.e., under proper boundary conditions they satisfy

$$(\mathcal{L}\phi, \psi) = (\phi, \mathcal{L}\psi), \quad (\psi, \mathcal{G}\psi) \leq 0, \quad \forall \phi, \psi \in L^2(\Omega). \quad (2.6)$$

Therefore, the gradient flow system (2.5) satisfies the following energy dissipation law

$$\frac{dF}{dt} = \left(\mathcal{L}\phi + \frac{\delta g}{\delta \phi}, \partial_t \phi \right) = \left(\mathcal{L}\phi + \frac{\delta g}{\delta \phi}, \mathcal{G} \left(\mathcal{L}\phi + \frac{\delta g}{\delta \phi} \right) \right) \leq 0. \quad (2.7)$$

2.2 Model reformulation using the SAV approach

For simplicity of notations, we assume g only depends on ϕ , but not its spatial derivatives. But we note the SAV approach works for a more general g . We first introduce a scalar auxiliary variable

$$q(t) = \sqrt{(g(\phi), 1) + C_0}, \quad (2.8)$$

where C_0 is a positive number such that $(g(\phi), 1) + C_0 > 0$. Then we can reformulate the original gradient flow system (2.5) into the following equivalent PDEs

$$\begin{cases} \partial_t \phi = \mathcal{G} \left(\mathcal{L}\phi + \frac{qg'(\phi)}{\sqrt{(g(\phi), 1) + C_0}} \right), \\ \partial_t q = \left(\frac{g'(\phi)}{2\sqrt{(g(\phi), 1) + C_0}}, \partial_t \phi \right), \end{cases} \quad (2.9)$$

with the consistent initial condition

$$q|_{t=0} = \sqrt{(g(\phi|_{t=0}), 1) + C_0}. \quad (2.10)$$

It is obvious that the new system (2.9) along with the consistent initial condition (2.10) is equivalent to the original gradient flow system (2.5). So in our latter discussion, we are going to design arbitrarily high-order numerical approximations for the equivalent model (2.9), which in turn solves the original gradient flow problem (2.5).

In the reformulated system (2.9), the modified free energy could be defined as

$$E = \frac{1}{2} (\mathcal{L}\phi, \phi) + q^2 - C_0, \quad (2.11)$$

which is equal to the free energy F of the original system (2.5) in the continuous level, by noticing (2.8). As we have been emphasizing, the free energy of the equivalent system (2.9) is a quadratic functional with respect to the new variables. And the new system (2.9) satisfies the modified energy dissipation law

$$\begin{aligned} \frac{dE}{dt} &= (\mathcal{L}\phi, \phi_t) + 2qq_t = \left(\mathcal{L}\phi + \frac{qg'(\phi)}{\sqrt{(g(\phi), 1) + C_0}}, \phi_t \right) \\ &= \left(\mathcal{L}\phi + \frac{qg'(\phi)}{\sqrt{(g(\phi), 1) + C_0}}, \mathcal{G} \left(\mathcal{L}\phi + \frac{qg'(\phi)}{\sqrt{(g(\phi), 1) + C_0}} \right) \right) \leq 0. \end{aligned} \quad (2.12)$$

Next we will focus on the SAV reformulated system (2.9)-(2.10) to develop arbitrarily high-order unconditionally energy stable numerical approximations, which in turn solve (2.5).

3 High Order Time Discretization

In this section, we first derive the RK method and the collocation method in time for the SAV reformulated system (2.9), respectively. Then both a class of RK methods and the collocation methods with the Gaussian quadrature nodes are proved to preserve the corresponding energy dissipation law and thus unconditionally energy stable. Note that the proposed methods can reach arbitrarily high order while preserving the modified energy dissipation law.

Applying an s -stage RK method to solve the system (2.9), we obtain the following HSAV-RK scheme.

Scheme 3.1 (s -stage HSAV-RK Method). *Let b_i, a_{ij} ($i, j = 1, \dots, s$) be real numbers and let $c_i = \sum_{j=1}^s a_{ij}$. For given (ϕ^n, q^n) , the following intermediate values are first calculated by*

$$\begin{aligned} \Phi_i &= \phi^n + \Delta t \sum_{j=1}^s a_{ij} k_j, \\ Q_i &= q^n + \Delta t \sum_{j=1}^s a_{ij} l_j, \\ k_i &= \mathcal{G} \left(\mathcal{L}\Phi_i + \frac{Q_i g'(\Phi_i)}{\sqrt{(g(\Phi_i), 1) + C_0}} \right) \\ l_i &= \left(\frac{g'(\Phi_i)}{2\sqrt{(g(\Phi_i), 1) + C_0}}, k_i \right). \end{aligned} \quad (3.1)$$

Then (ϕ^{n+1}, q^{n+1}) is updated via

$$\begin{aligned} \phi^{n+1} &= \phi^n + \Delta t \sum_{i=1}^s b_i k_i, \\ q^{n+1} &= q^n + \Delta t \sum_{i=1}^s b_i l_i. \end{aligned} \quad (3.2)$$

The RK coefficients are usually displayed by a Butcher table

$$\frac{\mathbf{cA}}{\mathbf{b}^T} \left| \begin{array}{c} c_1 a_{11} \cdots a_{1s} \\ \vdots \\ c_s a_{s1} \cdots a_{ss} \\ \hline b_1 \cdots b_s \end{array} \right|,$$

where $\mathbf{A} \in \mathbb{R}^{s,s}$, $\mathbf{b} \in \mathbb{R}^s$, and $\mathbf{c} = \mathbf{A}\mathbf{l}$ with $\mathbf{l} = (1, 1, \dots, 1)^T \in \mathbb{R}^s$.

For general HSAV-RK methods, we have the following energy-stability theorem.

Theorem 3.1. *If the coefficients of an HSAV-RK method satisfy*

$$b_i a_{ij} + b_j a_{ji} = b_i b_j, \quad b_i \geq 0, \quad \forall i, j = 1, \dots, s, \quad (3.3)$$

then it is unconditionally energy stable, i.e., it satisfies the following energy dissipation law

$$E^{n+1} - E^n = \Delta t \sum_{i=1}^s b_i \left(\mathcal{L}\Phi_i + \frac{Q_i g'(\Phi_i)}{\sqrt{(g(\Phi_i), 1) + C_0}}, \mathcal{G} \left[\mathcal{L}\Phi_i + \frac{Q_i g'(\Phi_i)}{\sqrt{(g(\Phi_i), 1) + C_0}} \right] \right) \leq 0, \quad (3.4)$$

where $E^n = \frac{1}{2}(\mathcal{L}\phi^n, \phi^n) + (q^n)^2 - C_0$.

Proof. Denoting $\phi^{n+1} = \phi^n + \Delta t \sum_{i=1}^s b_i k_i$ and noticing that the operator \mathcal{L} is linear and self-adjoint, we have

$$\frac{1}{2}(\mathcal{L}\phi^{n+1}, \phi^{n+1}) - \frac{1}{2}(\mathcal{L}\phi^n, \phi^n) = \Delta t \sum_{i=1}^s b_i (k_i, \mathcal{L}\phi^n) + \frac{\Delta t^2}{2} \sum_{i,j=1}^s b_i b_j (k_i, \mathcal{L}k_j). \quad (3.5)$$

Applying $\phi^n = \Phi_i - \Delta t \sum_{j=1}^s a_{ij} k_j$ to the right of (3.5), we can deduce

$$\frac{1}{2}(\mathcal{L}\phi^{n+1}, \phi^{n+1}) - \frac{1}{2}(\mathcal{L}\phi^n, \phi^n) = \Delta t \sum_{i=1}^s b_i (k_i, \mathcal{L}\Phi_i), \quad (3.6)$$

where $\sum_{i,j=1}^s b_i a_{ij} (k_i, \mathcal{L}k_j) = \sum_{i,j=1}^s b_j a_{ji} (k_i, \mathcal{L}k_j)$ and $b_i a_{ij} + b_j a_{ji} = b_i b_j$ were used. Similarly, we have

$$|q^{n+1}|^2 - |q^n|^2 = 2\Delta t \sum_{i=1}^s b_i l_i Q_i = \Delta t \sum_{i=1}^s b_i \left(\frac{Q_i g'(\Phi_i)}{\sqrt{(g(\Phi_i), 1) + C_0}}, k_i \right). \quad (3.7)$$

Adding (3.6) and (3.7) leads to

$$E^{n+1} - E^n = \Delta t \sum_{i=1}^s b_i \left(\mathcal{L}\Phi_i + \frac{Q_i g'(\Phi_i)}{\sqrt{(g(\Phi_i), 1) + C_0}}, k_i \right). \quad (3.8)$$

Replacing $k_i = \mathcal{G} \left(\mathcal{L}\Phi_i + \frac{Q_i g'(\Phi_i)}{\sqrt{(g(\Phi_i), 1) + C_0}} \right)$ to (3.8), we can arrive at (3.4). This completes the proof. \square

Applying an s -stage collocation method for the system (2.9), we obtain the following HSAV-Collocation scheme.

Scheme 3.2 (s -stage HSAV Collocation Method). *Let c_1, \dots, c_s be distinct real numbers ($0 \leq c_i \leq 1$). For given (ϕ^n, q^n) , the collocation polynomials $u(t)$ and $v(t)$ is two polynomials of degree s satisfying*

$$u(t_n) = \phi^n, \quad v(t_n) = q^n, \quad (3.9)$$

$$\partial_t u(t_n^i) = \mathcal{G} \left(\mathcal{L}u(t_n^i) + \frac{v(t_n^i)g'(u(t_n^i))}{\sqrt{(g(u(t_n^i)), 1) + C_0}} \right), \quad (3.10)$$

$$\partial_t v(t_n^i) = \left(\frac{g'(u(t_n^i))}{2\sqrt{(g(u(t_n^i)), 1) + C_0}}, \partial_t u(t_n^i) \right), \quad (3.11)$$

where $t_n^i = t_n + c_i \Delta t$ and $i = 1, \dots, s$. And then the numerical solution is defined by $\phi^{n+1} = u(t_n + \Delta t)$ and $q^{n+1} = v(t_n + \Delta t)$.

Theorem 1.4 on page 31 of [23] indicates that the collocation method yields a special RK method. If the collocation points c_1, \dots, c_s are chosen as the Gaussian quadrature nodes, i.e., the zeros of the s -th shifted Legendre polynomial $\frac{d^s}{dx^s} (x^s(x-1)^s)$, Scheme 3.2 is called the Gaussian collocation method. Based on the Gaussian quadrature nodes, the interpolating quadrature formula has order $2s$, and the Gaussian collocation method shares the same order $2s$. For instance, the RK coefficients of fourth order and sixth order HSAV schemes are given explicitly below (see [23] for coefficients of higher orders).

$\begin{array}{c} \frac{1}{2} - \frac{\sqrt{3}}{6} \quad \frac{1}{4} \quad \frac{1}{4} - \frac{\sqrt{3}}{6} \\ \frac{1}{2} + \frac{\sqrt{3}}{6} \quad \frac{1}{4} + \frac{\sqrt{3}}{6} \quad \frac{1}{4} \\ \hline \frac{1}{2} \quad \frac{1}{2} \end{array}$	$\begin{array}{c} \frac{1}{2} - \frac{\sqrt{15}}{10} \quad \frac{5}{36} \quad \frac{2}{9} - \frac{\sqrt{15}}{15} \quad \frac{5}{36} - \frac{\sqrt{15}}{30} \\ \frac{1}{2} \quad \frac{5}{36} + \frac{\sqrt{15}}{24} \quad \frac{2}{9} \quad \frac{5}{36} - \frac{\sqrt{15}}{24} \\ \frac{1}{2} + \frac{\sqrt{15}}{10} \quad \frac{5}{36} + \frac{\sqrt{15}}{30} \quad \frac{2}{9} + \frac{\sqrt{15}}{15} \quad \frac{5}{36} \\ \hline \frac{5}{18} \quad \frac{4}{9} \quad \frac{5}{18} \end{array}$
---	--

Table 3.1: RK coefficients of Gaussian collocation methods of order 4 and 6.

For conservative systems with quadratic invariants, the Gaussian collocation methods have been proven to conserve the corresponding discrete quadratic invariants [23]. Here we show that they are also unconditionally energy stable for dissipative systems with quadratic free energy.

Theorem 3.2. *The s -stage HSAV Gaussian collocation Scheme 3.2 is unconditionally energy stable, i.e., it satisfies the following energy dissipation law*

$$\begin{aligned} & E^{n+1} - E^n \\ &= \Delta t \sum_{i=1}^s b_i \left(\mathcal{L}u(t_n^i) + \frac{v(t_n^i)g'(u(t_n^i))}{\sqrt{(g(u(t_n^i)), 1) + C_0}} \right), \mathcal{G} \left[\mathcal{L}u(t_n^i) + \frac{v(t_n^i)g'(u(t_n^i))}{\sqrt{(g(u(t_n^i)), 1) + C_0}} \right] \\ & \leq 0, \end{aligned} \quad (3.12)$$

where $E^n = \frac{1}{2}(\mathcal{L}\phi^n, \phi^n) + (q^n)^2 - C_0$ and $t_n^i = t_n + c_i \Delta t$, c_i ($i = 1, \dots, s$) are the Gaussian quadrature nodes, $b_i \geq 0$ ($i = 1, \dots, s$) are the Gauss-Legendre quadrature weights, $u(t), v(t)$ are the collocation polynomial of the Gaussian collocation methods.

Proof. Noticing $\phi^n = u(t_n), q^n = v(t_n)$ and $\phi^{n+1} = u(t_{n+1}), q^{n+1} = v(t_{n+1})$, we have

$$\begin{aligned} E^{n+1} - E^n &= \frac{1}{2}(\mathcal{L}\phi^{n+1}, \phi^{n+1}) - \frac{1}{2}(\mathcal{L}\phi^n, \phi^n) + (q^{n+1})^2 - (q^n)^2 \\ &= \frac{1}{2}(u(t_{n+1}), \mathcal{L}u(t_{n+1})) - \frac{1}{2}(u(t_n), \mathcal{L}u(t_n)) + |v(t_{n+1})|^2 - |v(t_n)|^2 \end{aligned}$$

$$\begin{aligned}
&= \int_{t_n}^{t_{n+1}} \left[\frac{1}{2} \frac{d}{dt} (u(t), \mathcal{L}u(t)) + \frac{d}{dt} |v(t)|^2 \right] dt \\
&= \int_{t_n}^{t_{n+1}} \left[(\dot{u}(t), \mathcal{L}u(t)) + 2\dot{v}(t)v(t) \right] dt.
\end{aligned}$$

The integrand $(\dot{u}(t), \mathcal{L}u(t))$ and $\dot{v}(t)v(t)$ are polynomial of degree $2s - 1$, which is integrated without error by the s -stage Gaussian quadrature formula. It therefore follows from the collocation condition that

$$\begin{aligned}
&\int_{t_n}^{t_{n+1}} \left[(\dot{u}(t), \mathcal{L}u(t)) + 2\dot{v}(t)v(t) \right] dt \\
&= \Delta t \sum_{i=1}^s b_i \left[(\dot{u}(t_n^i), \mathcal{L}u(t_n^i)) + 2\dot{v}(t_n^i)v(t_n^i) \right] \\
&= \Delta t \sum_{i=1}^s b_i \left(\dot{u}(t_n^i), \mathcal{L}u(t_n^i) + \frac{v(t_n^i)g'(u(t_n^i))}{\sqrt{(g(u(t_n^i)), 1) + C_0}} \right) \\
&= \Delta t \sum_{i=1}^s b_i \left(\mathcal{L}u(t_n^i) + \frac{v(t_n^i)g'(u(t_n^i))}{\sqrt{(g(u(t_n^i)), 1) + C_0}}, \mathcal{G} \left[\mathcal{L}u(t_n^i) + \frac{v(t_n^i)g'(u(t_n^i))}{\sqrt{(g(u(t_n^i)), 1) + C_0}} \right] \right) \leq 0,
\end{aligned}$$

which leads to (3.12). This completes the proof. \square

Remark 3.1. *The proposed high-order energy stable schemes don't depend on the specific form of the mobility \mathcal{G} and the effective free energy F , i.e., they work for all the gradient flow models (2.1).*

Remark 3.2. *At each time step, even though solving an HSAV scheme takes longer than solving the SAV scheme, much larger time step size could be used for the HSAV scheme than the SAV scheme to reach the same accuracy (due to the high-order accuracy of the HSAV scheme). Overall, for simulations reaching similar accuracy, the HSAV scheme will take less CPU time than the SAV scheme, making the HSAV scheme superior for long time dynamic simulations.*

4 Spatial discretization

To make the order of accuracy in space compatible with the arbitrarily high-order in time, we employ the Fourier pseudospectral method in space for Scheme 3.1 and Scheme 3.2 to arrive at fully discrete HSAV-RK methods and fully discrete HSAV collocation methods. Then the fully discrete HSAV-RK methods with (3.3) and the fully discrete HSAV Gaussian collocation methods can be proved similarly to preserve the corresponding energy dissipation law in the fully discrete level.

Firstly, we recall the two-dimensional Fourier pseudospectral method [5, 16]. To make the paper self-explanatory, we briefly reintroduce the following notations (see [16] for more details). Let N_x, N_y be two positive even integers. The spatial domain $\Omega = [0, L_x] \times [0, L_y]$ is uniformly partitioned with mesh size $h_x = L_x/N_x, h_y = L_y/N_y$ and

$$\Omega_h = \{(x_j, y_k) | x_j = jh_x, y_k = kh_y, 0 \leq j \leq N_x - 1, 0 \leq k \leq N_y - 1\}.$$

Let $V_h = \{u | u = \{u_{j,k} | (x_j, y_k) \in \Omega_h\}\}$ be the space of grid functions on Ω_h . For any two vector grid functions $\mathbf{v} = (u_m), \mathbf{v} = (v_m)$ ($u_m, v_m \in V_h$), define the discrete inner

product and norm as follows

$$(\mathbf{v}, \mathbf{v})_h = h_x h_y \sum_m \sum_{j=0}^{N_x-1} \sum_{k=0}^{N_y-1} (u_m)_{j,k} (v_m)_{j,k}, \quad \|\mathbf{v}\|_h = \sqrt{(\mathbf{v}, \mathbf{v})_h}.$$

We define

$$S_N = \text{span}\{X_j(x)Y_k(y), j = 0, 1, \dots, N_x - 1; k = 0, 1, \dots, N_y - 1\}$$

as the interpolation space, where $X_j(x)$ and $Y_k(y)$ are trigonometric polynomials of degree $N_x/2$ and $N_y/2$, given respectively by

$$X_j(x) = \frac{1}{N_x} \sum_{m=-N_x/2}^{N_x/2} \frac{1}{a_m} e^{im\mu_x(x-x_j)}, \quad (4.1)$$

$$Y_k(y) = \frac{1}{N_y} \sum_{m=-N_y/2}^{N_y/2} \frac{1}{b_m} e^{im\mu_y(y-y_k)}, \quad (4.2)$$

where

$$a_m = \begin{cases} 1, & |m| < N_x/2, \\ 2, & |m| = N_x/2, \end{cases} \quad b_m = \begin{cases} 1, & |m| < N_y/2, \\ 2, & |m| = N_y/2, \end{cases}$$

and $\mu_x = 2\pi/L_x, \mu_y = 2\pi/L_y$. We define the interpolation operator $I_N : C(\Omega) \rightarrow S_N$ as follows:

$$I_N u(x, y) = \sum_{j=0}^{N_x-1} \sum_{k=0}^{N_y-1} u_{j,k} X_j(x) Y_k(y), \quad (4.3)$$

where $u_{j,k} = u(x_j, y_k)$. The key of spatial Fourier pseudospectral discretization is to obtain derivative $\partial_x^{s_1} \partial_y^{s_2} I_N u(x, y)$ at collocation points. Then, we differentiate (4.3) and evaluate the resulting expressions at point (x_j, y_k) as follows

$$\partial_x^{s_1} \partial_y^{s_2} I_N u(x_j, y_k) = \sum_{m_1=0}^{N_x-1} \sum_{m_2=0}^{N_y-1} u_{m_1, m_2} (\mathbf{D}_{s_1}^x)_{j, m_1} (\mathbf{D}_{s_2}^y)_{k, m_2},$$

where $\mathbf{D}_{s_1}^x$ and $\mathbf{D}_{s_2}^y$ are $N_x \times N_x$ and $N_y \times N_y$ matrices, respectively, with elements given by

$$(\mathbf{D}_{s_1}^x)_{j, m} = \frac{d^{s_1} X_m(x_j)}{dx^{s_1}}, \quad (\mathbf{D}_{s_2}^y)_{k, m} = \frac{d^{s_2} Y_m(y_k)}{dy^{s_2}}.$$

Define three operators \odot , \otimes and \oslash as follows:

$$(u \odot v)_{j,k} = u_{j,k} v_{j,k}, \quad (\mathbf{A} \otimes \mathbf{B} u)_{j,k} = \sum_{m=0}^{N_x-1} \mathbf{A}_{j,m} u_{m,k}, \quad (\mathbf{B} \oslash u)_{j,k} = \sum_{m=0}^{N_y-1} \mathbf{B}_{k,m} u_{j,m},$$

where $u, v \in V_h$. It is easy to show that these three operators possess the following properties:

$$u \odot v = v \odot u, \quad \mathbf{A} \otimes \mathbf{B} \oslash u = \mathbf{B} \oslash \mathbf{A} \otimes u, \quad \mathbf{A} \oslash \mathbf{B} \oslash u = (\mathbf{A} \mathbf{B}) \oslash u, \quad \oslash = \otimes \text{ or } \oslash.$$

Then we have

$$\partial_x^{s_1} \partial_y^{s_2} I_N u(x_j, y_k) = (\mathbf{D}_{s_1}^x \otimes \mathbf{D}_{s_2}^y \oslash u)_{j,k}.$$

Lemma 4.1 ([14]). *Denote*

$$\mathbf{A}_{\alpha,s} = \begin{cases} \left[i\mu_{\alpha} \text{phdiag} \left(0, 1, \dots, \frac{N_{\alpha}}{2} - 1, 0, -\frac{N_{\alpha}}{2} + 1, \dots, -1 \right) \right]^s, & \text{phwhen } s \text{ phodd,} \\ \left[i\mu_{\alpha} \text{phdiag} \left(0, 1, \dots, \frac{N_{\alpha}}{2} - 1, \frac{N_{\alpha}}{2}, -\frac{N_{\alpha}}{2} + 1, \dots, -1 \right) \right]^s, & \text{phwhen } s \text{ pheven,} \end{cases} \quad \alpha = x \text{ or } y,$$

we have

$$\mathbf{D}_s^{\alpha} = F_{N_{\alpha}}^{-1} \mathbf{A}_{\alpha,s} F_{N_{\alpha}}, \quad (4.4)$$

where $F_{N_{\alpha}}$ is the discrete Fourier transform, and $F_{N_{\alpha}}^{-1}$ is the discrete inverse Fourier transform.

Lemma 4.2. *For real matrix $\mathbf{A} \in \mathbb{R}_{N_{pha} \times N_{pha}}$, $pha = x$ or y , and $u, v \in V_h$,*

$$(\mathbf{A} @ u, v)_h = (u, \mathbf{A}^T @ v)_h. \quad (4.5)$$

Using identity (4.5), anti-symmetry of \mathbf{D}_{2s-1}^a and symmetry of \mathbf{D}_{2s}^a , $\forall a \in \{x, y\}, s \in \mathbb{Z}^+$, we obtain

$$\left(\mathbf{D}_{2s-1}^a @ u, v \right)_h = - \left(u, \mathbf{D}_{2s-1}^a @ v \right)_h, \quad \left(\mathbf{D}_{2s}^a @ u, v \right)_h = \left(u, \mathbf{D}_{2s}^a @ v \right)_h,$$

which implies that the Fourier pseudospectral method preserves discrete integration-by-parts formulae. Here we note that the retention of discrete integration-by-parts formulae is the key to constructing the spatial structure-preserving algorithm because the properties of the operators \mathcal{L} and \mathcal{G} are defined by the integration-by-parts formulae. Therefore, we can apply the Fourier pseudospectral method to obtain the corresponding discrete self-adjoint operator \mathcal{L}_h and the negative semi-definite operator \mathcal{G}_h , i.e., they satisfy

$$(\mathcal{L}_h \phi, \psi)_h = (\phi, \mathcal{L}_h \psi)_h, \quad (\psi, \mathcal{G}_h \psi)_h \leq 0, \quad \forall \phi, \psi \in V_h. \quad (4.6)$$

Applying the Fourier pseudospectral method for Scheme 3.1, we obtain the following fully discrete scheme.

Scheme 4.1 (Fully Discrete HSAV-RK Method). *Let b_i, a_{ij} ($i, j = 1, \dots, s$) be real numbers and let $c_i = \sum_{j=1}^s a_{ij}$. For given $\phi^n \in V_h$ and q^n , the following intermediate values are first calculated by*

$$\begin{aligned} \Phi_i &= \phi^n + \Delta t \sum_{j=1}^s a_{ij} k_j, \\ Q_i &= q^n + \Delta t \sum_{j=1}^s a_{ij} l_j, \\ k_i &= \mathcal{G}_h \left(\mathcal{L}_h \Phi_i + \frac{Q_i g'(\Phi_i)}{\sqrt{(g(\Phi_i), 1)_h + C_0}} \right) \\ l_i &= \left(\frac{g'(\Phi_i)}{2\sqrt{(g(\Phi_i), 1)_h + C_0}}, k_i \right)_h, \end{aligned} \quad (4.7)$$

where $\Phi_i, k_i \in V_h$. Then $\phi^{n+1} \in V_h$, q^{n+1} is updated via

$$\begin{aligned} \phi^{n+1} &= \phi^n + \Delta t \sum_{i=1}^s b_i k_i, \\ q^{n+1} &= q^n + \Delta t \sum_{i=1}^s b_i l_i. \end{aligned} \quad (4.8)$$

Applying the Fourier pseudospectral method for Scheme 3.2, we obtain the following fully discrete scheme.

Scheme 4.2 (Fully Discrete HSAV Collocation Method). *Let c_1, \dots, c_s be distinct real numbers ($0 \leq c_i \leq 1$). For given $\phi^n \in V_h$ and q^n , $u(t)$ is a $N_x \times N_y$ matrix polynomial of degree s and $v(t)$ is a polynomial of degree s satisfying*

$$u(t_n) = \phi^n, \quad v(t_n) = q^n, \quad (4.9)$$

$$\dot{u}(t_n^i) = \mathcal{G}_h \left(\mathcal{L}_h u(t_n^i) + \frac{v(t_n^i)g'(u(t_n^i))}{\sqrt{(g(u(t_n^i)), 1)_h + C_0}} \right), \quad (4.10)$$

$$\dot{v}(t_n^i) = \left(\frac{g'(u(t_n^i))}{2\sqrt{(g(u(t_n^i)), 1)_h + C_0}}, \dot{u}(t_n^i) \right)_h, \quad (4.11)$$

where $t_n^i = t_n + c_i \Delta t$ and $i = 1, \dots, s$. And then the numerical solution is defined by $\phi^{n+1} = u(t_n + \Delta t)$ and $q^{n+1} = v(t_n + \Delta t)$.

Similarly, we have the following theorems.

Theorem 4.1. *If the coefficients of a fully discrete HSAV-RK method satisfy*

$$b_i a_{ij} + b_j a_{ji} = b_i b_j, \quad b_i \geq 0, \quad \forall i, j = 1, \dots, s, \quad (4.12)$$

then it is unconditionally energy stable, i.e., it satisfies the following energy dissipation law

$$E_h^{n+1} - E_h^n = \Delta t \sum_{i=1}^s b_i \left(\mathcal{L}_h \Phi_i + \frac{Q_i g'(\Phi_i)}{\sqrt{(g(\Phi_i), 1)_h + C_0}}, \mathcal{G}_h \left[\mathcal{L}_h \Phi_i + \frac{Q_i g'(\Phi_i)}{\sqrt{(g(\Phi_i), 1)_h + C_0}} \right] \right)_h \leq 0, \quad (4.13)$$

where $E_h^n = \frac{1}{2}(\mathcal{L}_h \phi^n, \phi^n)_h + (q^n)^2 - C_0$.

Theorem 4.2. *The fully discrete HSAV Gaussian collocation Scheme 4.2 is unconditionally energy stable, i.e., it satisfies the following energy dissipation law*

$$\begin{aligned} & E_h^{n+1} - E_h^n \\ = & \Delta t \sum_{i=1}^s b_i \left(\mathcal{L}_h u(t_n^i) + \frac{v(t_n^i)g'(u(t_n^i))}{\sqrt{(g(u(t_n^i)), 1)_h + C_0}}, \mathcal{G}_h \left[\mathcal{L}_h u(t_n^i) + \frac{v(t_n^i)g'(u(t_n^i))}{\sqrt{(g(u(t_n^i)), 1)_h + C_0}} \right] \right)_h \\ & \leq 0. \end{aligned} \quad (4.14)$$

where $E_h^n = \frac{1}{2}(\mathcal{L}_h \phi^n, \phi^n)_h + (q^n)^2 - C_0$ and $t_n^i = t_n + c_i \Delta t$, c_i ($i = 1, \dots, s$) are the Gaussian quadrature nodes, $b_i \geq 0$ ($i = 1, \dots, s$) are the Gauss-Legendre quadrature weights.

As the proofs of Theorem 4.1 and 4.2 are similar with their semi-discrete version as shown in Theorem 3.1 and 3.2, we thus omit the details for simplicity.

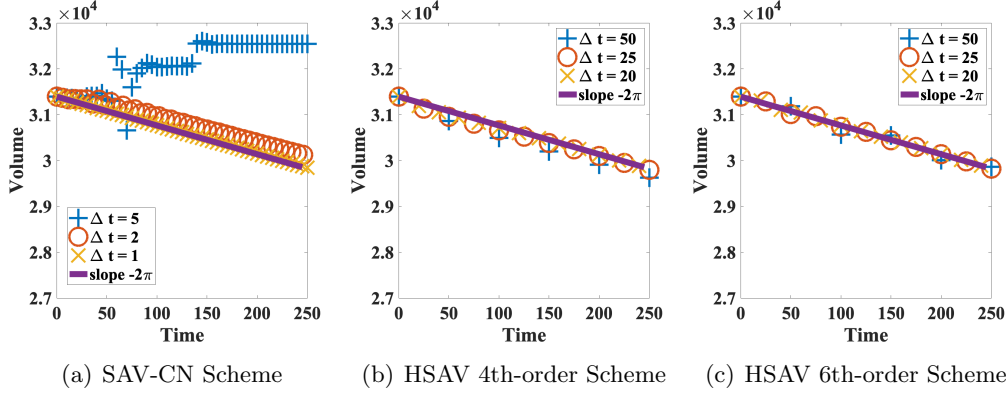


Fig. 5.1: Benchmark problem for the Allen-Cahn equation. This figure shows the volume of the disk decreasing with time with different schemes and various time steps.

5 Numerical examples

In this section, we conduct several numerical tests to verify the theoretical results in the previous section. We emphasize that the newly proposed HSAV schemes could reach arbitrarily high order accuracy in time (with proper choice of the Gaussian collocation points), and they are all unconditionally energy stable. For simplicity, in the rest of this paper, we only use 4th and 6th order for demonstration purpose. Moreover, the CPU time is calculated with a 3.2 GHz Intel Core i7 using Matlab R2018b on MacOS Mojave version 10.14.2.

Example 1: the Allen-Cahn equation. First of all, we test the proposed numerical schemes for solving the widely-used Allen-Cahn (AC) equation [1]. Mainly, the AC equation is proposed as

$$\partial_t \phi = -M \left(-\varepsilon^2 \Delta \phi + (\phi^3 - \phi) \right), \quad (5.1)$$

where M is the mobility parameter and ε controls the interfacial thickness. We choose the broadly embraced benchmark problem [7], i.e. set the initial profile for ϕ as:

$$\phi(x, y, t = 0) = \begin{cases} 1, & x^2 + y^2 < 100^2, \\ -1, & x^2 + y^2 \geq 100^2, \end{cases} \quad (5.2)$$

which is a disk centered at the origin, and use the domain $[-128 \ 128]^2$. The parameters are chosen as $M = \varepsilon = 1$. It is known that the area of the disk will shrink, following the linear dynamics $V = \pi R_0^2 - 2\pi t$ asymptotically, with R_0 the initial radius. Here we test the dynamics using the proposed HSAV schemes. The numerical results are summarized in Figure 5.1. We observe that the HSAV schemes can use much larger time step to capture the correct volume shrinking dynamics than the classical SAV schemes.

Example 2: the Cahn-Hilliard equation. Next, we study the widely-used Cahn-Hilliard equation with the Ginzburg-Landau free energy. Specifically, given the Ginzburg-Landau free energy $F = (-\frac{\varepsilon^2}{2} \Delta \phi, \phi) + (\frac{1}{4}(1 - \phi^2)^2, 1)$ and constant mobility λ , the model is proposed as

$$\partial_t \phi = \lambda \Delta \left[-\varepsilon^2 \Delta \phi + (\phi^3 - \phi) \right]. \quad (5.3)$$

If we set $\mathcal{G} = \lambda \Delta$, $\mathcal{L} = -\varepsilon^2 \Delta + \gamma_0$ and $g(\phi) = \frac{1}{4}(1 - \phi^2)^2 - \gamma_0 \phi^2 + \frac{C_0}{|\Omega|}$, where C_0 is a constant such that $(g, 1) > 0$. By introducing the scalar auxiliary variable $q = \sqrt{(g, 1)}$,

the Cahn-Hilliard equation (5.3) could be rewritten as the reformulated gradient flow form of (2.9)

$$\begin{aligned}\partial_t \phi &= \lambda \Delta \left[-\varepsilon^2 \Delta \phi + \gamma_0 \phi + \frac{q}{\sqrt{(g,1)}} g' \right], \\ \partial_t q &= \left(\frac{g'}{2\sqrt{(g,1)}}, \partial_t \phi \right),\end{aligned}\tag{5.4}$$

with the consistent initial condition for q , i.e. $q(t=0) = \sqrt{(g,1)}|_{t=0}$.

First of all, we conduct a time-step refinement test to verify the accuracy of our proposed high order schemes. We choose the domain as $[0, 1] \times [0, 1]$ and spatial meshes $N_x = N_y = 256$. The parameters are chosen as $\lambda = 10^{-3}$, $\varepsilon = 0.01$, $\gamma_0 = 1$, $C_0 = 1$. The initial profile for ϕ is given as $\phi(x, y, t=0) = \sin(2\pi x) \sin(2\pi y)$. Both the SAV Crank-Nicolson (SAV-CN) scheme (see [39, 38]) and the newly proposed HSAV Scheme 3.2 with fourth order and sixth order collocation points are tested. The numerical errors in L^2 norm at $t = 1$ are summarized in Figure 5.2. We observe that the two HSAV schemes reach the fourth and sixth order accuracy respectively. In particular, the L^2 errors of HSAV schemes are significantly (in several orders of magnitudes) smaller than the SAV-CN scheme.

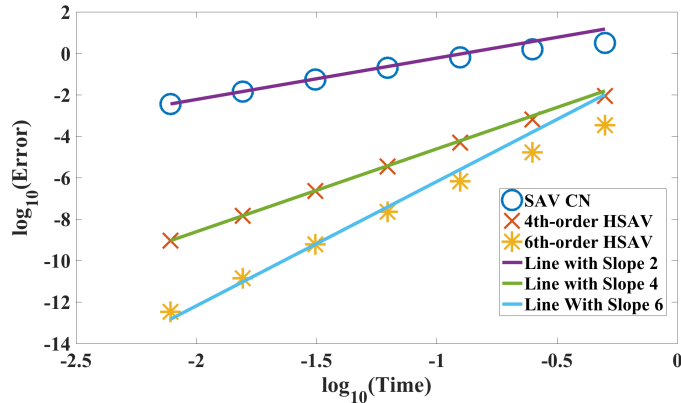


Fig. 5.2: Time refinement test for the SAV schemes solving the Cahn-Hilliard equation. This figure demonstrates the HSAV scheme can reach its high-order accuracy. And its numerical error is dramatically smaller than the SAV-CN scheme.

In addition, to assure the L^2 norm of the numerical error for ϕ at $t = 1$ smaller than 10^{-10} , the approximately minimum time steps are $\delta t = 10^{-5}$ for the SAV scheme, $\delta t = 0.004$ for the HSAV 4th-order scheme, $\delta t = 0.02$ for the HSAV 6th-order scheme. The total CPU time is summarized in Table 5.1, where we observe the HSAV scheme takes much less CPU time than the SAV scheme. It indicates the HSAV schemes are superior to the SAV schemes for accurate long-time dynamic simulations.

Table. 5.1: Total CPU time using various numerical schemes solving the CH model.

SAV Scheme	HSAV 4th-order Scheme	HSAV 6th-order Scheme
δt	0.00001	0.025 0.02
CPU time (seconds)	165.32	3.00 2.62

Next we compare the different SAV schemes for simulating the coarsening dynamics of two-phase immiscible fluids using the Cahn-Hilliard equation in (5.3). We choose the domain as $[0, 4\pi] \times [0, 4\pi]$ and use meshes $N_x = N_y = 512$. The parameters are chosen

as $\lambda = 0.1$, $\epsilon = 0.025$, $\gamma_0 = 1$, $C_0 = 1$. And we use an initial profile of ϕ as

$$\phi(x, y, t = 0) = 0.001rand(x, y), \quad (5.5)$$

where $rand(x, y)$ generates random number between -1 and 1 . The predicted energy evolution using different SAV schemes with various time steps are summarized in Figure 5.3. We observe that for the SAV-CN scheme, it can predict the correct energy evolution with time step $\Delta t = 0.00025$ (where the predicted energy evolution with time step $\Delta t = 0.0005$ is noticeably inaccurate). For the fourth order HSAV scheme, it can predict accurate energy evolution even with time step $\Delta t = 0.05$; and for the sixth order HSAV scheme, it even works well with time step $\Delta t = 0.1$, which is more than 10^3 bigger than the one with the SAV-CN scheme.

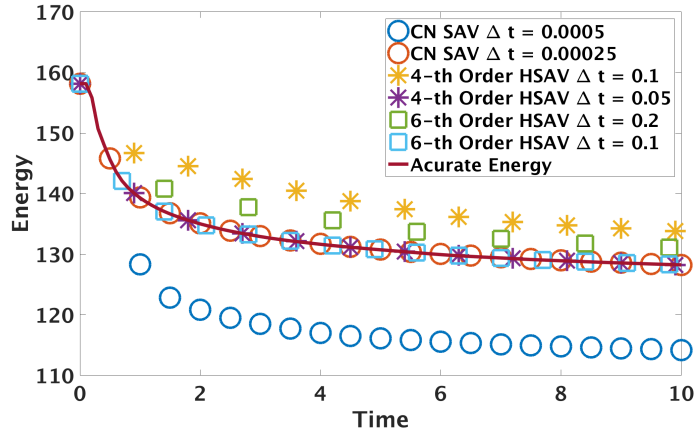


Fig. 5.3: A comparison of energy evolution using different SAV numerical schemes with various time steps. This figure illustrates the HSAV scheme could predict accurate energy evolution with much larger time steps than the SAV-CN scheme.

Then we use the HSAV schemes to conduct the long-time dynamic simulations of coarsening. We use the same parameters as above, and choose the initial profile

$$\phi(x, y, t = 0) = \phi_0 + 10^{-3}rand(x, y), \quad (5.6)$$

where ϕ_0 is a constant and $rand(x, y)$ generates a random number in the range of -1 to 1 . Then we choose $\phi_0 = 0, 0.1, 0.5$. We use the sixth order HSAV scheme with the time step $\Delta t = 0.1$. The simulation results are summarized in Figure 5.4, where we present the profile of ϕ at different times. We can observe the HSAV schemes can capture the phase transition dynamics accurately even with such time step time size. In particular, when ϕ_0 is small, i.e., the two components have similar total volume, the spinodal decomposition takes effect. When the volume of one phase is dominant, (for instance, $\phi_0 = 0.5$), the nucleation takes effects. These findings are a strong agreement with reports in [13].

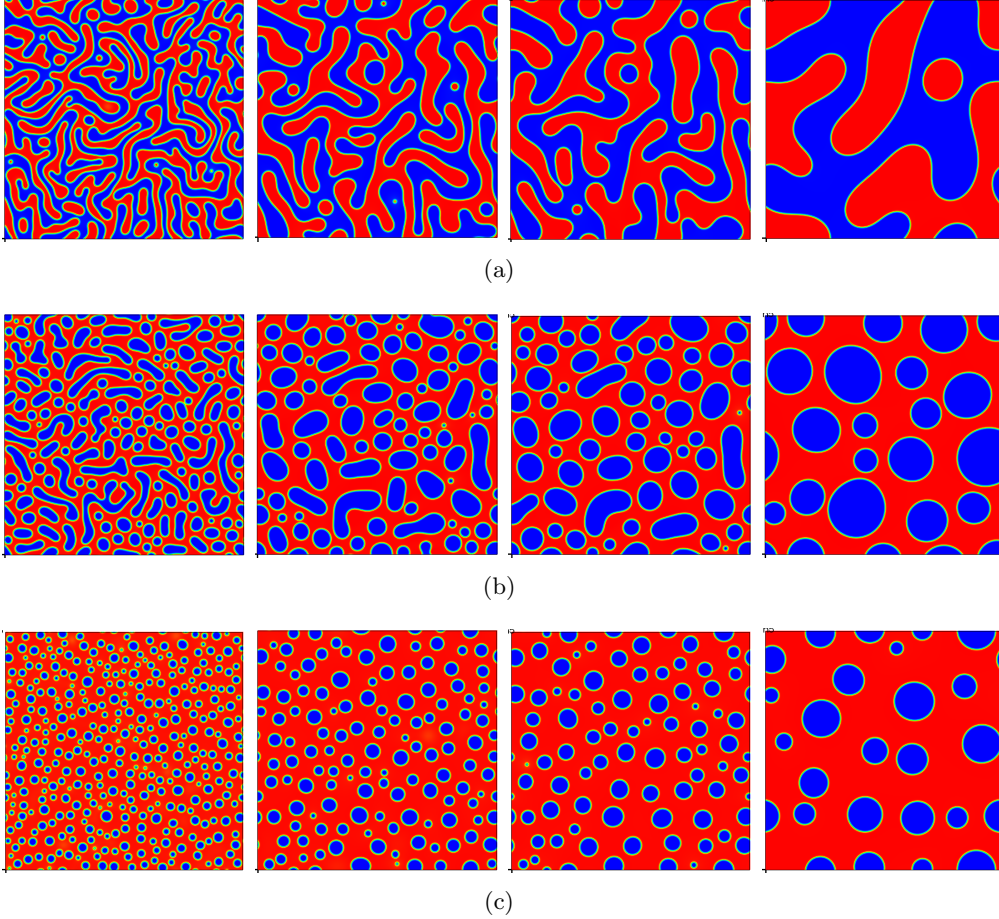


Fig. 5.4: Coarsening dynamics of two phase immiscible fluid using the 6th order HSAV scheme with time step $\Delta t = 0.1$. Here we choose $\phi_0 = 0, 0.1, 0.5$, and the results are shown in (a)-(c) respectively. This figure presents the profile of ϕ at time $t = 10, 50, 100, 1000$ for the simulation in Figure 5.3. It illustrates the HSAV scheme could capture the phase separation dynamics accurately even with large time step.

Next, we study the power-law coarsening dynamics. Here we set $\lambda = 0.02$, $\varepsilon = 0.05$, and domain $[0, 4\pi]^2$, and use the initial profile $\phi(x, y, t = 0) = 0.001 \text{rand}(-1, 1)$. It is known that the effective free energy decreases asymptotically following a power law $E(t) \approx O(t^{-1/3})$. We use the 4th, 6th order HSAV schemes and the SAV-CN scheme to calculate it, with 256^2 meshes and $\gamma_0 = 1$, $C_0 = 1$. The obtained results are summarized in Figure 5.5. We observe that all the numerical schemes can capture the power law dynamics very well when the time step is small enough, saying when $\delta t = 10^{-3}$. However, the maximum time step of capturing the correct dynamics using the HSAV scheme is much larger than that of the SAV-CN scheme.

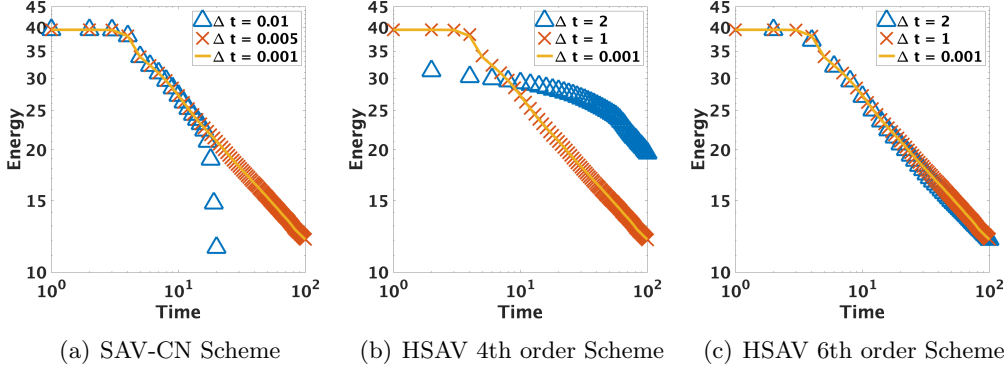


Fig. 5.5: The energy evolution with different time steps. Here the log-log scale of the energy with respect to time is plotted.

Example 3: The Molecular Beam Epitaxy Model. In the last case, we consider the molecular beam epitaxy (MBE) growth model without slope selection [42]. There is a huge amount of work in literature on investigating the MBE models analytically and numerically [42, 37, 34, 35, 9, 12, 26, 38, 49, 11, 45, 28, 30, 29].

Given the height profile of MBE denoted as ϕ , the evolution equation reads as

$$\partial_t \phi = -M \left(\varepsilon^2 \Delta^2 \phi + \nabla \cdot \left((1 - |\nabla \phi|^2) \nabla \phi \right) \right), \quad (5.7)$$

with periodic boundary condition. This model could be viewed as a L^2 gradient flow with respect to the effective free energy

$$F(\phi) = \int_{\Omega} \left(\frac{\varepsilon^2}{2} (\Delta \phi)^2 + \frac{1}{4} (|\nabla \phi|^2 - 1)^2 \right) d\mathbf{x}, \quad (5.8)$$

with a constant mobility M .

If we denote $\mathcal{G} = -M$, $\mathcal{L} = \varepsilon^2 \Delta^2 - \gamma_0 \Delta$ and $g(\nabla \phi) = \frac{1}{4} (|\nabla \phi|^2 - 1 - \gamma_0)^2 + \frac{C_0}{|\Omega|}$, and introduce the scalar auxiliary variable

$$q = \sqrt{(g, 1)}, \quad (5.9)$$

and the intermediate function

$$H(\nabla \phi) = \frac{\nabla \cdot \left((\gamma_0 + 1 - |\nabla \phi|^2) \nabla \phi \right)}{2 \sqrt{\int_{\Omega} \frac{1}{4} (|\nabla \phi|^2 - 1 - \gamma_0)^2 d\mathbf{x} + C_0}}, \quad (5.10)$$

the equation can be reformulated as

$$\begin{aligned} \partial_t \phi &= -M \left(\varepsilon^2 \Delta^2 \phi - \gamma_0 \Delta \phi + 2qH \right), \\ \partial_t q &= \left(H, \partial_t \phi \right), \end{aligned} \quad (5.11)$$

with the consistent initial condition for q , i.e. $q(t=0) = \sqrt{(g, 1)}|_{t=0}$.

First of all, we would like to test the convergence rate for our proposed scheme. Following the strategy in example 1, we use Cauchy sequences, where the errors are calculated as the differences between numerical solutions with adjacent time steps. We set $M = 1$, $\varepsilon = 1$ and the domain $[0, 2\pi]^2$. We use a smooth initial condition $\phi(x, y, 0) = \sin(x) \sin(y)$, and choose $\gamma_0 = 1$, $C_0 = 1$, 256^2 meshes. The refinement-test results are

summarized in Figure 5.6. We observe that all the schemes reach their expected orders of convergence when the time-step is small enough. However, the HSAV schemes have dramatically smaller numerical errors (with several magnitudes smaller) than the SAV-CN scheme, which highlights the advantages of the newly proposed HSAV schemes.

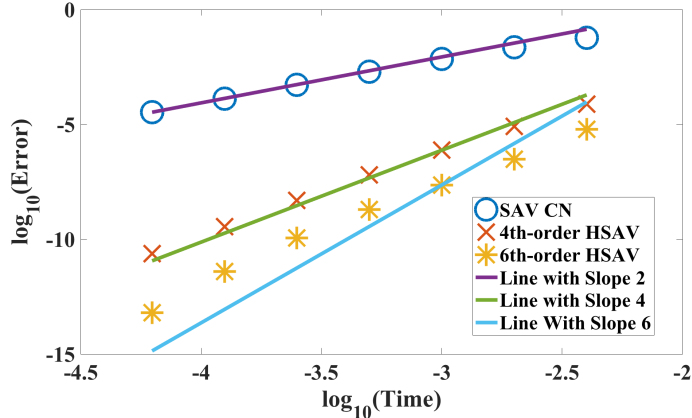


Fig. 5.6: Time refinement test for the SAV schemes. This figure demonstrates the HSAV scheme can reach its high-order accuracy. And its numerical error is dramatically smaller than the SAV-CN schemes.

Then, the proposed 4th-order and 6th-order HSAV schemes are tested via a benchmark problem [49], Consider the domain $[0, 2\pi]^2$, and parameters $\varepsilon^2 = 0.1$, $M = 1$. We pick the initial profile

$$\phi(x, y, t = 0) = 0.1(\sin(3x) \sin(2y) + \sin(5x) \sin(5y)).$$

This is a classic example that has been studied intensively [42, 6]. The effective free energy dynamics using different schemes with various time steps are plotted. We notice that even though all schemes assure the energy dissipation properties, the SAV-CN scheme requires a much smaller time step size (around $\delta t = 10^{-4}$) to predict accurate energy dissipation. In the meanwhile, the HSAV scheme could predict energy evolution accurately even with the time step $\delta t = 0.05$, which is 500 larger than the SAV scheme.

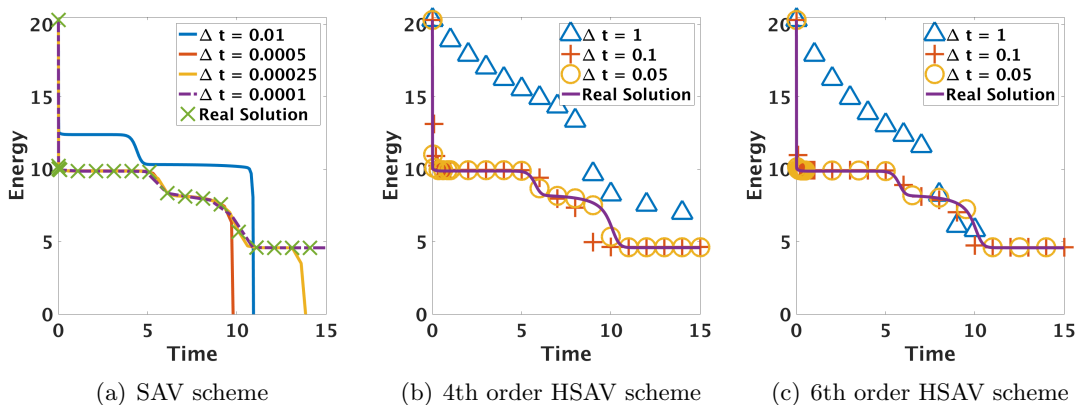


Fig. 5.7: Energy evolution calculated by different SAV schemes with various time step sizes. This figure demonstrates the HSAV scheme could predict accurate energy dissipation dynamics with much larger time steps than the SAV scheme while solving the MBE model with slope selection.

Besides, the total CPU times using each scheme to calculate the MBE model till $t = 15$ is summarized in Table 5.2, where we observe the HSAV scheme is much faster than the SAV scheme, as much larger time steps can be used for HSAV scheme while preserving the desired accuracy.

Table. 5.2: Total CPU time using various numerical schemes solving the MBE model.

	SAV-CN Scheme	HSAV 4th-order Scheme	HSAV 6th-order Scheme
δt	0.0001	0.025	0.05
CPU time (seconds)	672.39	79.45	74.72

One simulation using fourth order HSAV scheme with the time step $\delta t = 0.025$ is shown in Figure 5.8, where the height profile of ϕ at different times are shown. The patterns agree very well with other numerical solvers in literature, while we could use an extremely larger time step than the time-step used in other literature.

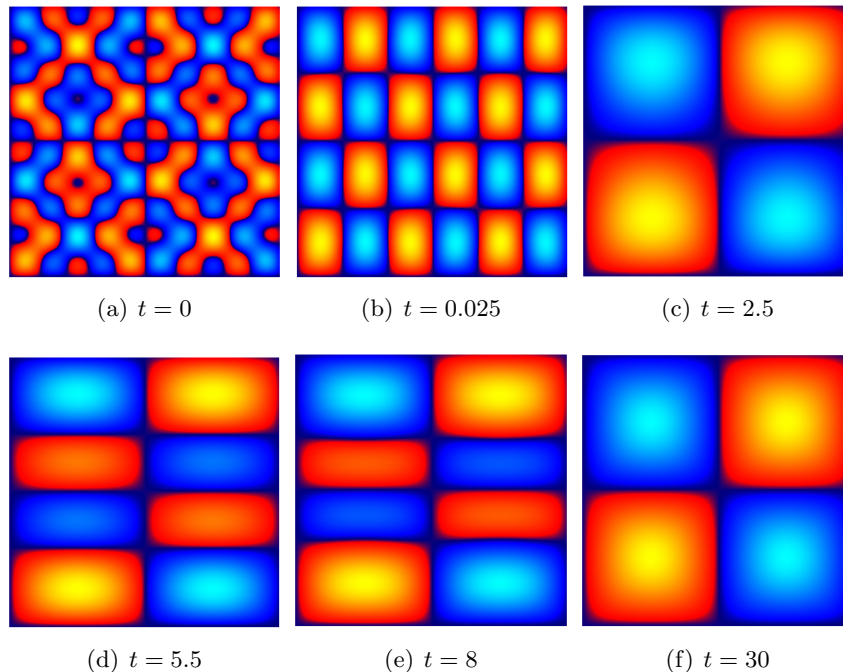


Fig. 5.8: The isolines of numerical solutions of the height function ϕ for the MBE model with slope selection using the 4th order HSAV scheme. The time step is $\delta t = 0.025$. Snapshots are taken at $t = 0, 0.05, 2.5, 5.5, 8, 30$, respectively.

6 Conclusion

In this paper, we combine the SAV approach with the structure-preserving discretization to propose a new class of energy stable methods for gradient flow models, which we name it the HSAV scheme. The proposed HSAV scheme could reach arbitrarily high-order accuracy in time while respecting the discrete energy dissipation law in term of the modified free energy of the SAV equivalent system. Therefore, the proposed schemes can be used to conduct longtime dynamic simulations for gradient flow problems with larger time steps. Some numerical benchmarks are presented to illustrate the excellent performance of the proposed numerical methods. Note that the proposed HSAV method is rather general to be applied for any gradient flow models derived through energy vari-

ation. Furthermore, it could also be generalized to study thermodynamically-consistent hydrodynamic models, which will be pursued in our later research.

Acknowledgment

Yuezheng Gong's work is partially supported by the Natural Science Foundation of Jiangsu Province (Grant No. BK20180413) and the National Natural Science Foundation of China (Grant No. 11801269). Jia Zhao's work is partially supported by National Science Foundation under grant number NSF DMS-1816783.

References

- [1] S. M. Allen and J. W. Cahn. Ground state structures in ordered binary alloys with second neighbor interactions. *Acta Metall.*, 20(423), 1972.
- [2] V. E. Badalassi, H. D. Ceniceros, and S. Banerjee. Computation of multiphase systems with phase field models. *Journal of Computational Physics*, 190(2):371–397, 2003.
- [3] F. Boyer and C. Lapuerta. Study of a three component cahn-hilliard flow model. *ESAIM: Mathematical Modeling and Numerical Analysis*, 40:653–687, 2006.
- [4] J. W. Cahn and J. E. Hilliard. Free energy of a nonuniform system. I. interfacial free energy. *Journal of Chemical Physics*, 28:258–267, 1958.
- [5] J. Chen and M. Qin. Multi-symplectic Fourier pseudospectral method for the nonlinear Schrödinger equation. *Electronic Transactions on Numerical Analysis*, 12:193–204, 2001.
- [6] L. Chen, J. Zhao, and X. Yang. Regularized linear schemes for the molecular beam epitaxy model with slope selection. *Applied Numerical Mathematics*, 128:138–156, 2018.
- [7] L. Q. Chen. Phase-field models for microstructure evolution. *Annual Review of Material Research*, 32(1):113–140, 2002.
- [8] W. Chen, S. Conde, C. Wang, X. Wang, and S. Wise. A linear energy stable scheme for a thin film model without slope selection. *Journal of Scientific Computing*, 52:546–562, 2012.
- [9] W. Chen, C. Wang, X. Wang, and S. M. Wise. A linear iteration algorithm for a second-order energy stable scheme for a thin film model without slope selection. *Journal of Scientific Computing*, 59(3):574–601, 2014.
- [10] D. J. Eyre. Unconditionally gradient stable time marching the Cahn-Hilliard equation. *Mrs Online Proceedings Library Archive*, 529:39–46, 1998.
- [11] W. Feng, C. Wang, and S. Wise. Linearly preconditioned nonlinear conjugate gradient solvers for the epitaxial thin film equation with slope selection. *arXiv*, pages 1–15, 2017.
- [12] W. Feng, C. Wang, S. Wise, and Z. Zhang. A second-order energy stable backward differentiation formula method for the epitaxial thin film equation with slope selection. *ArXiv*, page 1706.01943, 2017.

- [13] H. Gomez and T. J. R. Hughes. Provably unconditionally stable, second-order time-accurate, mixed variational methods for phase-field models. *Journal of Computational Physics*, 230(13):5310–5327, 2011.
- [14] Y. Gong, J. Cai, and Y. Wang. Multi-symplectic Fourier pseudospectral method for the Kawahara equation. *Communications in Computational Physics*, 16(1):35–55, 2014.
- [15] Y. Gong and J. Zhao. Energy-stable runge–kutta schemes for gradient flow models using the energy quadratization approach. *Applied Mathematics Letters*, 94:224–231, 2019.
- [16] Y. Gong, J. Zhao, and Q. Wang. Linear second order in time energy stable schemes for hydrodynamic models of binary mixtures based on a spatially pseudospectral approximation. *Advances in Computational Mathematics*, 44:1573–1600, 2018.
- [17] Y. Gong, J. Zhao, and Q. Wang. Second order fully discrete energy stable methods on staggered grids for hydrodynamic phase field models of binary viscous fluids. *SIAM J. Sci. Comput.*, 40(2):B528–B553, 2018.
- [18] Y. Gong, J. Zhao, X. Yang, and Q. Wang. Second-order linear schemes for hydrodynamic phase field models of viscous fluid flows with variable densities. *SIAM Journal on Scientific Computing*, 4(1):B138–B167, 2018.
- [19] B. Gonzalez-Ferreiro, H. Gomez, and I. Romero. A thermodynamically consistent numerical method for a phase field model of solidification. *Commun Nonlinear Sci Numer Simulat*, 19:2309–2323, 2014.
- [20] F. Guillen-Gonzalez and G. Tierra. On linear schemes for a Cahn-Hilliard diffuse interface model. *Journal of Computational Physics*, 234:140–171, 2013.
- [21] R. Guo and Y. Xu. Semi-implicit spectral deferred correction method based on the invariant energy quadratization approach for phase field problems. *Communication in Computational Physics*, 26(1):87–113, 2019.
- [22] Z. Guo, P. Lin, J. Lowengrub, and S. Wise. Mass conservative and energy stable finite difference methods for the quasi-incompressible navier-stokes-cahn-hilliard system: primitive variable and projection-type schemes. *Computer Methods in Applied Mechanics and Engineering*, 326:144–174, 2017.
- [23] E. Hairer, C. Lubich, and G. Wanner. *Geometric Numerical Integration: structure-preserving algorithms for ordinary differential equations*, volume 31. Springer, 2006.
- [24] D. Han, A. Brylev, X. Yang, and Z. Tan. Numerical analysis of second order, fully discrete energy stable schemes for phase field models of two phase incompressible flows. *Journal of Scientific Computing*, 70(3):965–989, 2017.
- [25] W. Hu and M. lai. Unconditionally energy stable immersed boundary method with application to vesicle dynamics. *East Asian Journal on Applied Mathematics*, 3(3):247–262, 2013.
- [26] L. Ju, X. Li, Z. Qiao, and H. Zhang. Energy stability and error estimates of exponential time differencing schemes for the epitaxial growth model without slope selection. *Mathematics of Computation*, 87(312):1859–1885, 2018.
- [27] Junseok Kim. Phase-field models for multi-component fluid flows. *Communication in Computational Physics*, 12(3):613–661, 2012.

- [28] R. V. Kohn and X. Yan. Upper bound on the coarsening rate for an epitaxial growth model. *Comm. Pure Appl. Math.*, 56:1549–1564, 2003.
- [29] B. Li and J. Liu. Epitaxial growth without slope selection: energetics, coarsening and dynamic scaling. *Journal of Nonlinear Science*, 14:429–451, 2004.
- [30] B. Li and J. G. Liu. Thin film epitaxy with or without slope selection. *European Journal of Applied Mathematics*, 14:713–743, 2003.
- [31] Y. Li, J. Kim, and N. Wang. An unconditionally energy-stable second-order time-accurate scheme for the cahn-hilliard equation on surfaces. *Commun Nonlinear Sci Numer Simulat*, 53:213–227, 2017.
- [32] L. Onsager. Reciprocal relations in irreversible processes I. *Physical Review*, 37:405–426, 1931.
- [33] L. Onsager. Reciprocal relations in irreversible processes II. *Physical Review*, 38:2265–2279, 1931.
- [34] Z. Qiao, Z. Sun, and Z. Zhang. Stability and convergence of second-order schemes for the nonlinear epitaxial growth model without slope selection. *Math. Comp.*, 84:653–674, 2015.
- [35] Z. Qiao, C. Wang, S. Wise, and Z. Zhang. Error analysis of a finite difference scheme for the epitaxial thin film model with slope selection with an improved convergence constant. *International Journal of Numerical Analysis and Modeling*, 14(2):1–23, 2017.
- [36] I. Romero. Thermodynamically consistent time-stepping algorithms for non-linear thermomechanical systems. *International Journal for Numerical Methods in Engineering*, 79:706–732, 2009.
- [37] J. Shen, C. Wang, X. Wang, and S. Wise. Second-order convex splitting schemes for gradient flows with Ehrlich-Schwoebel type energy: application to thin film epitaxy. *SIAM Journal of Numerical Analysis*, 50(1):105–125, 2012.
- [38] J. Shen, J. Xu, and J. Yang. A new class of efficient and robust energy stable schemes for gradient flows. *ArXiv*, page 1710.01331, 2017.
- [39] J. Shen, J. Xu, and J. Yang. The scalar auxiliary variable (sav) approach for gradient flows. *Journal of Computational Physics*, 353:407–416, 2018.
- [40] J. Shen and X. Yang. Numerical approximations of Allen-Cahn and Cahn-Hilliard equations. *Disc. Conti. Dyn. Sys.-A*, 28:1669–1691, 2010.
- [41] J. Shin, H. Lee, and J. Lee. Unconditionally stable methods for gradient flow using convex splitting runge-kutta scheme. *Journal of Computational Physics*, 347:367–381, 2017.
- [42] C. Wang, X. Wang, and S. Wise. Unconditionally stable schemes for equations of thin film epitaxy. *Discrete and Continuous Dynamic Systems*, 28(1):405–423, 2010.
- [43] C. Wang and S. Wise. An energy stable and convergent finite-difference scheme for the modified phase field crystal equation. *SIAM Journal on Numerical Analysis*, 49(3):945–969, 2011.

- [44] S. Wang, R. Sekerka, A. Wheeler, B. T. Murray, S. R. Coriell, R. J. Braun, and G. B. McFadden. Thermodynamically-consistent phase-field models for solidification. *Physica D*, 69:189–200, 1993.
- [45] C. Xu and T. Tang. Stability analysis of large time-stepping methods for epitaxial growth models. *SIAM Journal of Numerical Analysis*, 44(4):1759–1779, 2006.
- [46] X. Yang, J. Li, G. Forest, and Q. Wang. Hydrodynamic theories for flows of active liquid crystals and the generalized onsager principle. *Entropy*, 18(6):202, 2016.
- [47] X. Yang and J. Zhao. On linear and unconditionally energy stable algorithms for variable mobility Cahn-Hilliard type equation with logarithmic Flory-Huggins potential. *Communications in Computational Physics*, 25:703–728, 2019.
- [48] X. Yang, J. Zhao, and X. He. Linear, second order and unconditionally energy stable schemes for the viscous cahn-hilliard equation with hyperbolic relaxation. *Journal of Computational and Applied Mathematics*, 343:80–97, 2018.
- [49] X. Yang, J. Zhao, and Q. Wang. Numerical approximations for the molecular beam epitaxial growth model based on the invariant energy quadratization method. *Journal of Computational Physics*, 333:102–127, 2017.
- [50] X. Yang, J. Zhao, Q. Wang, and J. Shen. Numerical approximations for a three components cahn-hilliard phase-field model based on the invariant energy quadratization method. *Mathematical Models and Methods in Applied Sciences*, 27:1993–2023, 2017.
- [51] J. Zhao, X. Yang, Y. Gong, X. Zhao, X. Yang, J. Li, and Q. Wang. A general strategy for numerical approximations of non-equilibrium models—part i thermodynamical systems. *International Journal of Numerical Analysis and Modeling*, 15(6):884–918, 2018.